Journal Pre-proof

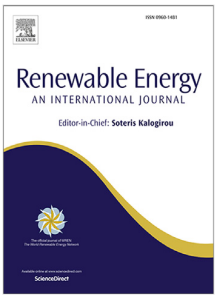

Performance of multi-stage tubular solar still operating under vacuum

W.L. Chen, G. Xie

PII: S0960-1481(22)01656-1
DOI: https://doi.org/10.1016/j.renene.2022.11.023
Reference: RENE 17968

To appear in: *Renewable Energy*

Received date : 6 April 2022
Revised date : 24 October 2022
Accepted date : 5 November 2022

Please cite this article as: W.L. Chen and G. Xie, Performance of multi-stage tubular solar still operating under vacuum, *Renewable Energy* (2022), doi: https://doi.org/10.1016/j.renene.2022.11.023.

This is a PDF file of an article that has undergone enhancements after acceptance, such as the addition of a cover page and metadata, and formatting for readability, but it is not yet the definitive version of record. This version will undergo additional copyediting, typesetting and review before it is published in its final form, but we are providing this version to give early visibility of the article. Please note that, during the production process, errors may be discovered which could affect the content, and all legal disclaimers that apply to the journal pertain.

© 2022 Elsevier Ltd. All rights reserved.

Journal Pre-proof

Renewable Energy, Volume 201, Part 2, December 2022, pp. 34-46
DOI:10.1016/j.renene.2022.11.023

Performance of multi-stage tubular solar still operating under vacuum

W.L. Chen[a], G. Xie[b,*]

[a] *School of Water, Energy and Environment, Cranfield University.*

[b] *State Key Laboratory of Hydraulics and Mountain River Engineering, College of Water Resource & Hydropower, Sichuan University, Chengdu 610065, China*

Abstract

Multi-stage solar desalination running under vacuum is a low-cost, effective and sustainable way to mitigate fresh water shortage. However, questions remain on the operation pressure (P_{op}) and stage number of the multi-stage solar still. To address these questions, a predictive model was developed for the yield of multi-stage tubular solar still under vacuum (MSSV) and validated against field experiments. A 3-stage tubular still under typical weather (i.e. 19.75 MJ/m^2 cumulative solar radiation) produced maximum water yield (7.15 kg/m^2) with optimal P_{op} (48 kPa), much higher than under normal (5.81 kg/m^2) and lower pressure (1.58 kg/m^2 with P_{op} = 20 kPa). At optimal P_{op}, a delicate balance exists between the energy adsorbed and dissipated. Stronger solar intensity leads to more water yield and higher optimal P_{op}, while increasing the stage number improved the fresh water yield with diminishing marginal effect and slightly shift the optimal P_{op} to a lower value. Using water immersion cooling other than air cooling significantly increased the water yield from 7.15 kg/m^2 to 10.51 kg/m^2. The MSSV model enriched the fundamental understanding of energy

*Corresponding author,2008xieguo@scu.edu.cn

Published by Elsevier. This is the Author Accepted Manuscript issued with: Creative Commons Attribution Non-Commercial No Derivatives License (CC:BY:NC:ND 4.0).
The final published version (version of record) is available online at DOI:10.1016/j.renene.2022.11.023. Please refer to any applicable publisher terms of use.

Journal Pre-proof

ultilization for solar desalination and could serve as a design tool to maximize the performance of multi-stage solar still by optimizing still parameters and geometry.

Keywords: Solar desalination, multi-stage, tubular solar still, vacuum, model, optimal pressure

1. Introduction

Freshwater scarcity becomes one of the most serious global challenges we face today [1]. 2.3 billion people are living in water-stressed countries as the latest UN water report indicated [2]. To alleviate water shortage, technological solutions such as the desalination were proposed to extract freshwater from saline water [3]. Amid all desalination technologies, the solar desalination was increasingly preferred by people living in remote and underdeveloped regions over traditional desalination technology such as the reverse osmosis (RO) [4, 5], for its advantage in light supporting system, portable installation [6] and the use of renewable clean solar energy [7, 8]. To provide a low-cost, sustainable solution for water scarcity, it is crucial to enhance the performance of the solar desalination.

Typical solar stills such as single basin solar still suffers from a low thermal efficiency in the range of 30-45%, and a freshwater productivity of less than 5 $L/m^2/day$ [9]. In this situation, conventional solar still was improved by enhancing the evaporation, diffusion and condensation of water in a desalination equipment [10, 11]. Various measures such as adding nanoparticles, adding

Journal Pre-proof

phase change material (PCM) and the solar-driven interfacial evaporation technology were proved to effectively enhance the water evaporation by increasing the heat absorption or reducing heat loss in the solar-thermal energy conversion process. Adding nanoparticles like Al2O3, TiO2 and CuO increased sunlight absorption of solar still [10], which led to a highest thermal efficiency of 50.34% (with 0.25% Al2O3) [12] and a higher productivity by 6% (with 2% nano-Cu) [13]. Alternatively, PCM stores thermal energy and compensates for the temporal mismatch between supply and demand for solar energy [14], and had shown to introduce 10% productive enhancement compared with conventional solar still [15, 16]. The recently developed solar-driven interfacial evaporation technology selectively heats the evaporative portion of water instead of the entire water in conventional solar still, and thus dramatically decrease heat loss and improve energy conversion efficiency of solar stills [17].

The performance of the solar still was also improved by enhancing the diffusion process of the generated vapor with techniques such as vacuum operation [18, 19]. For instance, an experimental study by Abakr and Ismail [20] obtained a production of 14.2 kg/m^2/day at 50 kPa, which was 45% higher than that at the atmospheric pressure [21]. Vacuum operation on a modified basin solar still led to enhancement of 16.2% and 29.7% in productivity and thermal efficiency, as revealed by the work of Ibrahim et al., [22]. A desalination system proposed by Hamawand et al., [23] produced yield up to 15 kg/m^2/day, while running under vacuum condition. A strikingly 100% increasing in productivity was achieved with a slight vacuum in the chamber, as revealed by the test of

Journal Pre-proof

Omara et al., [24]. Compare with basin solar stills, tubular solar still is more compact and owns a better pressure bearing capacity, thus more suitable to be operated under vacuum. In our previous studies, tubular solar still operating under vacuum was proved to be of high freshwater yield, thermal and economical efficiency. Vapor transportation within the tubular solar still under vacuum was then studied using computational fluid dynamics (CFD) model and visualization experiment [25] . Recently, we carried out a four-day outdoor experiment involving a three-effect tubular solar still operating under vacuum. At operating pressure of 95 (local atmospheric), 60, 40 and 20 kPa, the corresponding daily freshwater yields were 3.27, 6.323, 7.056 and 4.287 kg/m^2, and the corresponding energy utilization efficiencies were 0.77, 1.28, 1.39 and 0.88, respectively [26]. Various techniques were used to maintain a vacuum condition, i.e., vacuum pump [27], vacuum fan [24], vacuum spray dryer [23] and natural vacuum [28, 19].

Albeit the clear advantage and the wide application of vacuum operation in solar desalination, questions remain on the choice of stage number and the operational pressure. Study by Zheng et al., [29] with fixed electrical heating showed a better performance ratio of a three-effect still (i.e. 1.7) than a two-effect still (i.e. 1.4). Based on indoor experiments, Xie et al., [27] further proposed and evaluated a 5-effect modular desalination system composed of array tubular solar stills. Although the augment of yield by adding stages in basin solar still was proved by Karimi Estahbanati et al., [30], their experimental results also showed that lower bonus will be get in the higher stage. Moreover, adding more

Journal Pre-proof

stages in solar still will increase the fabrication cost, which implies that a solar still with excessive stages will suffer from a low economical performance. Accordingly, optimum number of stages for such tubular solar still operating under vacuum need to be further considered. Various operational pressure were recommended in the vacuum operation of solar still. A 50 kPa pressure was used in the experiment of Abakr et al., [20], whilst a extremely low pressure of 2-3 kPa was suggested by numerical studies of Reddy et al., [31, 32]. Their studies also suggested to adopt various operating pressure from 1.0 bar to 0.25 bar in different months, which could increase the distillate yield by nearly 200% [33]. The outdoor test by Xie et al., [26], on the other hand, suggested the optimum operation pressure in the range of 40 – 60 kPa.

In this study, we aim to investigate the yielding performance of multi-stage tubular solar still with different stages (1 – 6 stages) and operating under vacuum condition. First, a modified model was proposed for such solar still. Considering that buoyancy force due to concentration difference in the vacuum chamber would surpass that from thermal diffusion, the model was rebuilt on the basis of diffusion rule and the analogy between heat and mass transfer process inside an enclosure. Independent experimental data was selected to verify the reliability of the modified model, and evaluate the deviation. Next, the model was used to predict the yielding performance of the multi-stage still, and analyze the sensitivity to operation pressure. The optimal operation strategy of the still under different vacuum pressure and weather conditions was subsequently explored. The effect of ambient air temperature and the possibility of

Journal Pre-proof

extending the present model to other geometries were discussed in the end. This work is expected to be a guidance in optimizing the geometrical and operation parameters for the multi-stage solar still operating under vacuum condition.

2. Multi-stage tubular still

Fig. 1 shows the schematic of a TSS integrated with a solar collector and a vacuum pump, similar to the three-stage TSS in our previous study [38]. The distillation process under vacuum occurs in a multi-stage still chambers (denoted as #1, #2, #3, #4 and etc in Fig. 1), and the saline water in first stage is heated by circulating water (denoted as #0). Each stage has an independent tubular distillation chamber, where saline evaporates in the trough and generated vapor condensed on the shell. The condensate in each stage trickles down to the bottom and is collected in the freshwater tank. Except the first stage, saline water in other stages is heated by vapor in the inner adjacent stage. Repeatedly, thermal energy could be transferred from the inner to the outer stage. The exhaust heat is finally dissipated into the environment through the outer shell.

Heat transfer process of the multi-stage still could be seen in the right corner of Fig. 1. Solar energy is converted by collector and the circulating water deliver the heat to stage #1 (denoted as $Q_{hu,0}$). Generated vapor in stage #1 carries the latent heat, $Q_{e,1}$, to the upper space and is condensed on its inner surface. Besides evaporation, convection of the humid air also plays a role of the heat transportation, which is denoted as $Q_{c,1}$. Meanwhile, upper shell in stage #1 simultaneously receives the radiation heat ($Q_{r,1}$) from the evaporating surface.

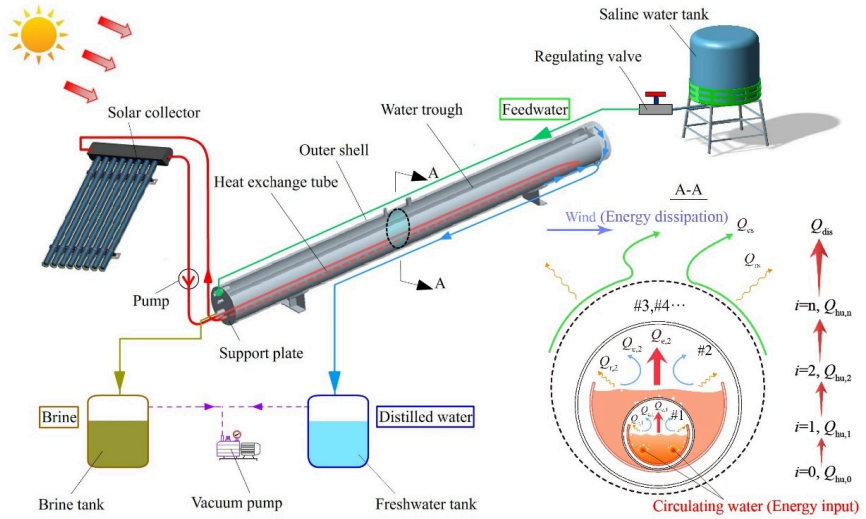

Figure 1: Schematic of the multi-stage tubular solar still operating under vacuum.

These three components ($Q_{e,1}, Q_{c,1}, Q_{r,1}$) constitute the heat resource for stage #2, which is denoted as $Q_{hu,1}$. Similar heat transfer process recurs in effects #2, #3 ($Q_{hu,2}, Q_{hu,3}$) until final heat (Q_{dis}) dissipates into the environment. The theoretical model for the above process was built with the following assumptions: 1) The condensation rate of vapor is equal to the evaporation rate in each stage; 2) Heat capacities of the shells and troughs are relatively small and are neglected in the calculation; 3) Heat loss through the two end plates is estimated to be less than 3% of total heat dissipation, and thus neglected in the calculation; 4) Leaking vapor through vacuum pump and the associated heat loss are neglected, except; (5) In case of still temperature reaches the saturation temperature of water at the operation pressure, the vapor generated are removed by the vacuum

Journal Pre-proof

pump; 6) Heat transfer through the trough wall is not taken in account.

3. Mathematical modelling of multi-stage still under vacuum

The model of multi-stage still operating under vacuum condition (MSSV) contains detailed mathematical description of heat and mass transfer of the still (§3.1 and §3.2). The analogy between heat and mass transfer at vacuum pressure differs from at normal pressure, and is discussed in §3.3. Finally, the thermophysical properties of humid air at vacuum pressure are present in §3.4.

The flowchart comparing the present and previous models was shown in Fig. 2. The most distinction can be observed with the different ways to calculate the distillate rate ($\dot{m}_e$). In Dunkle's model and Lewis relation, the rate is mainly determined by convective heat transfer coefficient (h_c), which is of good accuracy for cases at atmospheric pressure. By contrast, the present model is based on the specific correlations for vacuum distillation in [11], and could be more accurate for cases at $P_{op} \leq 60$ kPa. The corresponding distillate rate ($\dot{m}_e$) is derived from mass transfer coefficient (h_m), where buoyancy force arising from mass transfer will dominate the natural convection inside the cavity under vacuum.

3.1. heat transfer

3.1.1. Thermal energy balance in a multi-stage still

The schematic of energy transportation process inside the solar still with vertical ripple surface is also shown in Fig. 1. The heat source of the system

Journal Pre-proof

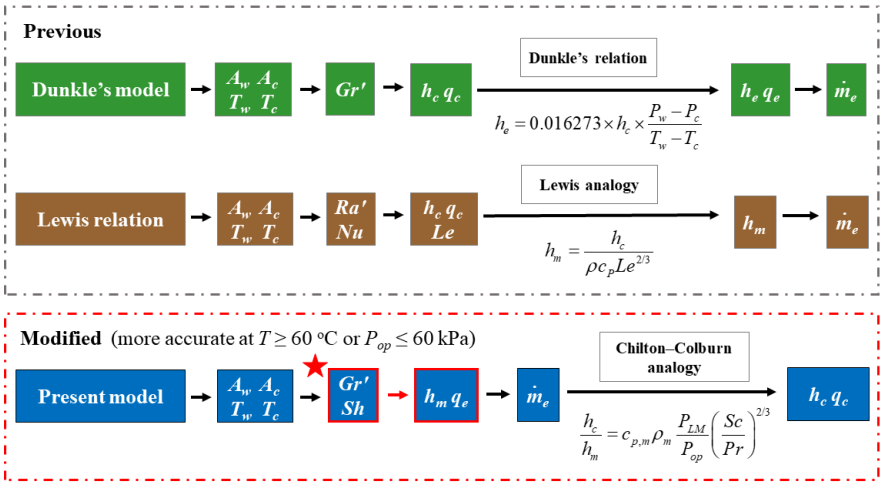

Figure 2: Flowchart of present and previous models.

is a concentrated anti-freezing solar collector (for environment tests), which is comprised of a vacuum tube and a absorbent surface. The solar energy is converted to thermal energy inside the vacuum tube. Subsequently, the heated water is introduced to the central water tank by a pump.

The energy balance of each stage reads

$$Q_{h,i} - Q_{k,i} - Q_{hu,i} = c_{p,w} M_i \frac{dT_i}{dt}. \tag{1}$$

For the interior stage (i stage, with $i \geq 1$) under steady condition, the input heat rate equals the output heat rate of $(i-1)$ stage, i.e., $Q_{h,i} = Q_{hu,i-1}$. No heat loss is considered inside the interior stage, i.e., $Q_{k,i} = 0$ for $i \geq 1$. The output heat rate $Q_{hu,i}$ for $i = 1, n-1$ is the summation of heat transferred by evaporation ($Q_{e,i}$), convection ($Q_{c,i}$) and radiation ($Q_{r,i}$), i.e.,

$$Q_{hu,i} = Q_{e,i} + Q_{c,i} + Q_{r,i}. \tag{2}$$

Journal Pre-proof

The evaporation rate is identical to the latent heat of the evaporated water mass, which can be expressed as

$$Q_{e,i} = h_{fg,i} h_{m,i} (\rho_{v,w,i} - \rho_{v,c,i}) A_{w,i}, \tag{3}$$

$\rho_{v,w,i}$ and $\rho_{v,c,i}$ refer to the density of vapor close to the water surface and condensation surface, respectively. The natural heat transferred by convection inside the i stage is calculated by Newton's cooling law:

$$Q_{c,i} = h_{c,w,i} A_{w,i} (T_{w,i} - T_{c,i}), \tag{4}$$

where the heat transfer coefficient of convection $h_{c,w,i}$ is obtained based on an analogy (to be further discussed in 3.3) between heat and mass transfer process. The radiation heat transfer between the evaporation and condensation surface is simplified as a radiation process between a rectangle plane and a half cylinder surface:

$$Q_{r,i} = \frac{\sigma (T_{w,i}^4 - T_{c,i}^4) A_{w,i}}{\frac{1}{\epsilon_w} + \frac{1-\epsilon_c}{\epsilon_c} \frac{A_{w,i}}{A_{c,i}/2}}, \tag{5}$$

where $\epsilon_w = 0.96$ and $\epsilon_c = 0.86$ are emissivities of water and the condensation surface.

3.1.2. Energy feed into the evaporation still

As shown in Fig. 1, the heat source of the system is the collected solar energy, which can be described as [34]

$$Q_{h,0} = G A_{co} \eta_{co}, \tag{6}$$

Journal Pre-proof

where $G(t)$ is the solar irradiance on the test day given by

$$G(t) = G_{max} \sin\left[\left(\frac{t - t_a}{t_b - t_a}\right)\pi\right], \tag{7}$$

with

$$G_{max} = \frac{H}{\int_{t_a}^{t_b} \sin\left[\left(\frac{t-t_a}{t_b-t_a}\right)\pi\right] \mathrm{d}t}. \tag{8}$$

The thermal efficiency η_{co} of a solar collector depends on the operating temperature and solar radiation flux. The η_{co} of the collector used in this experiment (purchased from ShenTai Ltd) was estimated by [26] as:

$$\eta_{co} = 0.635 - 1.96\frac{T_{w,0} - T_a}{G}. \tag{9}$$

The circulating water absorbs the solar energy and is heated, which then provides the heating rate of the first stage as the hot water flows into the central water tank. The energy transferred into the first stage by conduction and convection is recognized as the output energy for the $i = 0$ stage (i.e., $Q_{hu,0}$), and is given by

$$Q_{hu,0} = \frac{A_{es}}{\frac{\delta_0}{\lambda_{wall}} + \frac{1}{h_{c,0}} + \frac{1}{h_{c,1}}}(T_{w,0} - T_{w,1}), \tag{10}$$

with $h_{c,0}$ and $h_{c,a}$ being the heat transfer coefficient within and out of the exchange tube, A_{se} the surface area of exchange tube. The convective heat transfer coefficient $h_{c,0}$ is calculated by virtue of Dittus-Boelter formula

$$h_{c,0} = 0.023 Re_f^{0.8} Pr_f^{0.4}, \tag{11}$$

with $Re_f = \frac{v_{w,c} d_{se}}{\nu_w}$ and $Pr_f = \frac{\nu}{\alpha_w}$ are the Reynolds number and the Prandtl number respectively.

Journal Pre-proof

3.1.3. Energy dissipation

The energy dissipation occurs at both the lowest and last stage. For lowest stage, i.e., $i = 0$, the heat loss owing to conduction happens as the tube and solar collector with hot water exposing to the ambient cool air, which is calculated as

$$Q_{k,0} = A_0(T_{w,0} - T_a)/(R_1 + 1/(1/R_2 + 1/R_3)), \tag{12}$$

with $R_1 = \delta_{ins}/\lambda_{ins}$, $R_2 = 1/0.2787$ and $R_3 = 1/(5.7 + 3.8V_w)$ are the thermal resistance of insulation layer, outwall radiation and outwall convection (with V_w being the wind speed), respectively. A_0 is the total surface the connecting tubes. R_2 is calculated from

$$R_2 = \frac{1}{(T_{wall}^2 + T_{sky}^2)(T_{wall} + T_{sky})(\sigma\epsilon_{outwall})}. \tag{13}$$

T_{wall} is obtained through iteration. Note that $Q_{k,0}$ does not participate in the water evaporation or condensation, therefore $Q_{k,0}$ is considered as a net heat loss (i.e., $Q_{loss} = Q_{k,0}$).

In last stage, i.e., $i = n$, the energy dissipation due to radiation ($Q_{r,s}$) and convection ($Q_{c,s}$) from the tubular shell are considered,

$$Q_{dis} = Q_{c,s} + Q_{r,s}, \tag{14}$$

with

$$Q_{c,s} = A_{c,n}h_{c,s}(T_s - T_a), \tag{15}$$

and

$$Q_{r,s} = \epsilon_c\sigma A_{c,n}(T_s^4 - T_{sky}^4). \tag{16}$$

Journal Pre-proof

T_{sky} is given by Ahsan [35]

$$T_{sky} = 0.5T_a + 137.6. \tag{17}$$

$h_{c,s}$ is the convective heat transfer coefficient on outer side of the still shell which reads [36]:

$$h_{c,s} = \begin{cases} 5.7{+}3.8V_w & (V_w \leq 5\text{m/s}) \\ 6.15V_w^{0.8} & (V_w > 5\text{m/s}). \end{cases} \tag{18}$$

The thermal resistance of the shell is small compared to that of the convection outside the shell. Therefore, the temperature difference across the shell was neglected. Unlike $Q_{k,0}$, Q_{dis} is crucial for the evaporating and condensing of the water.

3.2. Mass Transfer

The mass transfer process in the distillation cavity consists the evaporation at the water surface and the condensation at the collecting surface. They reach balance in a very short time. Therefore, the mass transfer rate is essentially the evaporation capacity of water per square meter $\dot{m}_e$, and is given by

$$\dot{m}_e = h_m(\rho_{v,w} - \rho_{v,c}). \tag{19}$$

Using the expression of *Sherwood* number (Sh), the mass transfer coefficient h_m can be obtained as

$$h_m = Sh\frac{D_v}{L}. \tag{20}$$

Journal Pre-proof

The dependence of mass diffusion coefficient of water vapour (D_v) on the temperature and pressure is estimated as

$$D_v = D_0 \frac{P_0}{P_{op}} (\frac{T}{298})^{3/2}. \tag{21}$$

For the mass transfer process inside a semicircular distillation cavity under vaccum condition, an empirical correlation between *Sherwood* number (Sh), *Grashof* (Gr) number and *Schmidt* ($Sc = \frac{\mu}{D_v}$) number exists, i.e.

$$Sh = C(Gr.Sc)^x, \tag{22}$$

where $C = 0.46(P_0/P_{op})^{0.125}$ is obtained based on a group of experiments [11]. According to Adhikari [37], the value of x is either 0.25 for $Gr < 2.51 \times 10^5$ or 0.33 otherwise. In this case, the former value is taken.

In an enclosed space, the *Grashof* number given by

$$Gr = \frac{L^3 \rho_m^2 g \beta_m}{\mu_m^2} \Delta T \tag{23}$$

describes the natural convective heat transfer driven by the temperature difference $\Delta T = T_w - T_c$. Adhikari [37] suggested that the density variation in between vapour and air gives rise to an extra bouyancy force in driving the convection, and included this effect by revising the temperature difference in Eq.23 as

$$\Delta T' = \Delta T + \frac{P_w - P_c}{\frac{M_a P_{op}}{M_a - M_w} - P_w} T_w, \tag{24}$$

with P_w and P_c refer to the pressure of vapor close to water and condensation surface in each stage. The second term on the right hand of Eq.(24) thus accounts for the contribution of the diffusion process of vapour, and is becoming

Journal Pre-proof

much larger if the TSS is maintained at vacuum pressure other than atmospheric pressure. The *Grashof* number with revised temperature difference is used in this study.

As the water temperature approaching the saturation temperature ($T_{w,s}$), the vapor bubble forms within the water body (due to the high temperature) and contributes to the total mass transfer. These extra vapor bubble could not be captured by the expression for mass transfer based on natural evaporation, convection and concentration of water vapor. Since no expression was given for mass transfer under saturation pressure within solar still, an expression made use of Holman [38] was developed here, i.e.,

$$\dot{m}_e = C_{mb} \frac{D_v P_{op} M_v}{TRL} \log \frac{P_{op} - P_c}{P_{op} - P_w}, \tag{25}$$

with T, R and L being the stage temperature, the universal gas constant and the average distance between the evaporation and condensation surface respectively. Note that only diffusion transfer was considered in the expression of Holman [38]. A saturation coefficient (C_{mb}) is added to compensate the mass transfer owing to other mechanisms, i.e., convection and submerged boiling. The coefficient $C_{mb} = 2.5$ was obtained through a comparison with experimental data [27]. The transition of mass transfer from natural convection to saturation occurs while the water temperature reaches 0.5 K under the saturation temperature. A ramp up function was applied to ensure a smooth transition from mass transfer of normal condition to saturation, with a smooth window of 0.4 K. The mass

Journal Pre-proof

transfer under various condition is given as

$$\dot{m}_e = \begin{cases} \dot{m}_{e,1}, & T_{w,s} - T_w > 0.7, \\ \dot{m}_{e,1} \sin(\phi) + \dot{m}_{e,2} \cos(\phi), & 0.3 \leq T_{w,s} - T_w \leq 0.7, \\ \dot{m}_{e,2}, & T_{w,s} - T_w < 0.3, \end{cases} \tag{26}$$

where $\dot{m}_{e,1}$ and $\dot{m}_{e,2}$ are mass transfer under normal (Eq. 19) and saturation condition (Eq. 25), and $\phi = \frac{\pi}{4} \cdot (\frac{(T_{w,s} - T_w - 0.5)}{0.2} + 1)$. Therefore, the transition from $\dot{m}_{e,1}$ to $\dot{m}_{e,2}$ starts when the water temperature is 0.7 K below saturation temperature and terminates at 0.3 K below saturation temperature.

3.3. The analogy between heat and mass transfer at vacuum pressure

Theoretical study on the transport of heat and mass in the solar still enclosure was firstly performed by Dunkle [39], for typical average temperatures up to about 50 ^{o}C. A linear mixing relationship between h_m and $h_{c,w}$ was proposed. The validity of Dunkle's relation has been examined at a wide range of low and medium operational temperatures, but has shown to fail to predict mass transport with an adequate accuracy at high temperatures. Under Reynolds analogy assumption and low mass flux condition, Rahbar and Esfahani [40] adopted the Lewis relation to describe the h_m and $h_{c,w}$ relationship. However, at vacuum operation, considerable mass transfer rate is observed in the still even for medium temperature. The Reynolds analogy in particular the low mass flux condition is not usually satisfied for the circumstance of vacuum operation. Based on the Chilton-Colburn analogy which extends the validity of Reynolds analogy, Tsingliri [41] developed a predictive model that is also suitable for considerable

mass transfer, and is used in this study (see Fig. 3). Therefore, in the interior stage, i.e, for $1 \leq i \leq n$, the mass transfer coefficient $h_{m,i}$ and convective heat transfer coefficient $h_{c,w,i}$ satisfies

$$\frac{h_{c,w,i}}{h_{m,i}} = c_{p,m,i}\rho_{m,i}\frac{P_{LM,i}}{P_{op}}(\frac{Sc}{Pr})^{2/3}. \tag{27}$$

The logarithmic mean pressure of air P_{LM} reads [41]

$$P_{LM} = \frac{(P_c - P_w)}{\log((P_{op} - P_w)/(P_{op} - P_c))}. \tag{28}$$

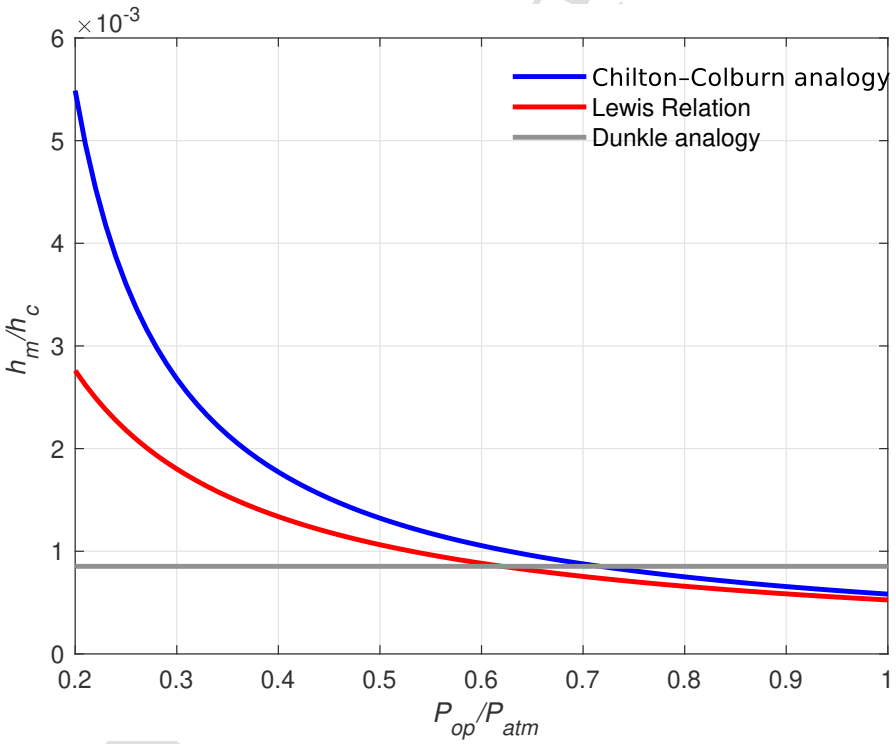

Figure 3: The analogy between heat and mass as a function of operating pressure. The temperature of the evaporation and condensation surface were 50 °C and 40 °C, respectively.

Journal Pre-proof

3.4. Thermophysical properties of humid air at vacuum pressure

The humid air inside the TSS at vacuum pressure is considered as a binary mixture of air and water vapour. Based on Dalton's law of partial pressure, the operating pressure P_{op} of the cavity is the sum of partial vapour pressure (P_v) and partial air pressure (P_a), i.e.,

$$P_{op} = P_v + P_a, \tag{29}$$

where P_v is given as

$$P_v = RH \cdot P_{sv}, \tag{30}$$

with RH being the relative humidity of vapor within the still. The saturation pressure (P_{sv}) of water between 0 and $100°C$ can be obtained from a temperature dependent empirical expression,

$$P_{sv} = A_0 + A_1 T_m + A_2 T_m^2 + A_3 T_m^3 + A_4 T_m^4, \tag{31}$$

with $A_0 = 1.131439334$, $A_1 = -3.750393331 \times 10^{-2}$, $A_2 = 5.591559189 \times 10^{-3}$, $A_3 = -6.220459433 \times 10^{-5}$ and $A_4 = 1.10581611 \times 10^{-6}$. As suggested by Tsilingiris [42], the humid air inside the TSS can be presumed to be saturated, which means $RH = 100\%$.

Journal Pre-proof

Journal Pre-proof

The thermophysical properties of the humid air are given as

$$M_m = M_a(1 - \frac{P_v}{P_{op}}) + M_v \frac{P_v}{P_{op}}, \tag{32}$$

$$\rho_m = \frac{P_{op} M_m}{R T_m}, \tag{33}$$

$$c_{p,m} = c_{p,a}(1 - \frac{P_v}{P_{op}}) \frac{M_a}{M_m} + c_{p,v} \frac{P_v}{P_{op}} \frac{M_v}{M_m}, \tag{34}$$

$$\lambda_m = \lambda_a(1 - \frac{P_v}{P_{op}}) + \lambda_v \frac{P_v}{P_{op}} \tag{35}$$

$$\mu_m = \frac{\mu_a(P_{op} - P_v)\sqrt{M_a} + \mu_v P_v \sqrt{M_v}}{(P_{op} - P_v)\sqrt{M_a} + P_v \sqrt{M_v}}. \tag{36}$$

4. Results

The MSSV model was firstly validated against two field experiments of stills with 3-effect operating under both normal and vacuum pressure (§4.1 and §4.2). The model was then used to examine the sensitivity of still performance on operational pressure (§4.3). Performance of still under various solar intensity was explored consequently with optimal operating strategies provided for various weather condition (§4.4). Finally, the effect of stages number was investigated (§4.5).

4.1. Temperature evolution

The MSSV model well reproduced the temperature evolution and fresh water yield of still operating under normal and vacuum pressure (see Fig.4 and .5). Under normal pressure, the temperature within the still increased in a sequential order, i.e., temperature of outer shell and waters in all stages followed the circulating water and increased one after another, indicating the direction

Journal Pre-proof

of heat transfer to be from circulating water to outer shell. The simulated peak temperature of water in circulating tube, stage 1 and stage 2 agree well with measure data. Water temperature in stage 1 closely follow the curve of circulating water until 18:00 when the energy input from solar irradiance faded away. After sunset, the simulated circulating water temperature quickly drops to lower than the temperature of outer shell, which contradicts the observation. This is due to the change of the direction of heat transfer. After sunset, the temperature of exposed parts of the system, i.e., outer shell, circulating water and the lowest stage, reduced to be lower than the inner part of the system. The reversed temperature gradient of circulating water and stage 1 leads to heat transfer from stage 1 to the circulating water and keeps the temperature of circulating water. This mechanism is not accounted for in the model. In the temperature rising period, there exists a time lag between the measured and simulated temperature, which is due to the duration time of vapor transportation in the experiments.

A strikingly flattened temperature curve was simulated for the first time for stills under vacuum operation see Fig. 5. The vacuum operation restricted the water temperature within the still to be lower or equal to the saturation temperature of water at the operating pressure. Consequently, flattened curves of water temperature (i.e., prolonged at peak temperature) were often observed for stills under vacuum operation but hadn't been simulated. In this study, the simulated water temperature of stage 1 stabilizes once reaching the saturation temperature. Meanwhile, water temperature in stage 2 and 3 experienced a

Journal Pre-proof

Journal Pre-proof

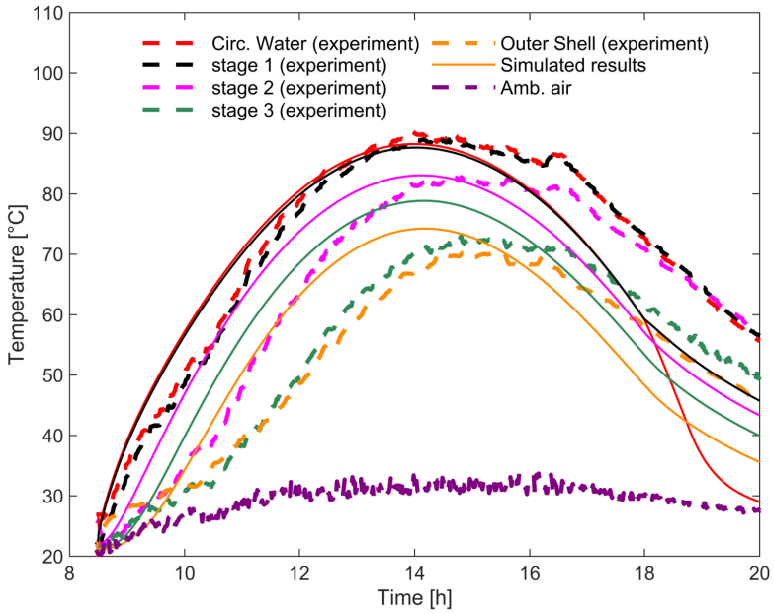

Figure 4: Comparison of simulation (solid lines) and experimental measurement (dashed lines), with $P_{op} = 95$ kPa, $G_{max} = 630\text{W/m}^2$ and $R_{sr} = 16.6$ MJ/m^2 (cumulative solar radiation). The simulated daily yield is 3.78 kg/m^2.

jump, due to the increased mass transfer under saturation, as explained in Eq. 25. The weather and temperature conditions of this experiment stand for typical conditions of vacuum operating solar still and was taken as a reference for later simulation.

4.2. Water yield prediction

A comparison regarding accumulated yield by different models was conducted, see Table 1. Under normal pressure (95 kPa), the present model pre-

Journal Pre-proof

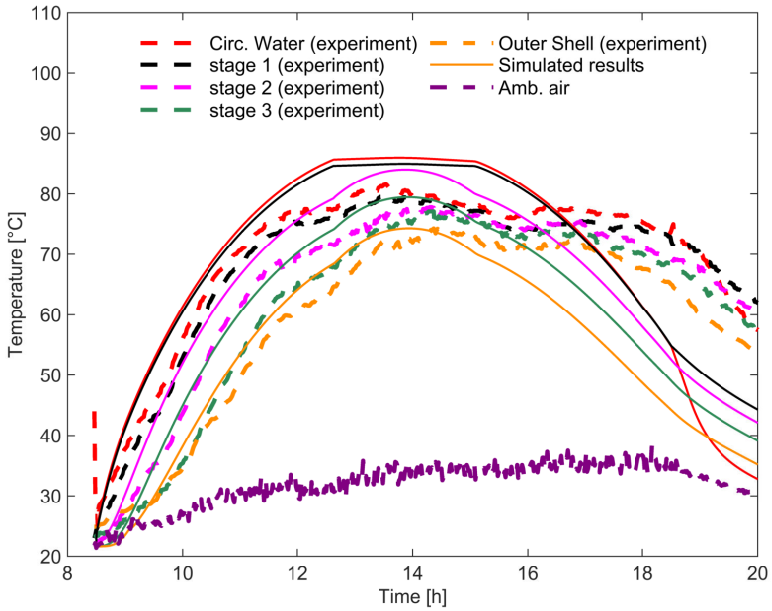

Figure 5: Comparison of simulation (solid lines) and experimental measurement (dashed lines), with $P_{op} = 60$ kPa, $G_{max} = 750\text{W/m}^2$ and $R_{sr} = 19.75$ MJ/m^2. The simulated daily yield is 6.32 kg/m^2.

dicted an accumulated water yield of 3.78 kg/m^2, which is slightly higher than that of the measured value, i.e., 3.27 kg/m^2 (see Table 1). With vacuum operation, the water yield predicted increases to 6.32 kg/m^2 and exactly matches the value measured (i.e. 6.32 kg/m^2). Model results were compared with other mathematical models [40], i.e., Dunkle's model and model based on Lewis relation in which the analogy between heat and mass transfer follows relations shown in Fig. 3. Note that in [40], the convective heat transfer coefficient was calculated from Nusselt number while mass transfer coefficient was then calcu-

Journal Pre-proof

Table 1: Comparison of measured yield and predicted values.

P_{op} (kPa)	Measured yield (kg/m^2)	Predicted yield (kg/m^2)			Deviation		
		Present	Dunkle	Lewis	Present	Dunkle	Lewis
95	3.27	3.78 (+15.6%)	3.00(-8.3%)	2.55(-22.0%)	15.6%	-8.3%	-22%
60	6.32	6.32	4.76	4.58	0%	-24.7%	-27.5%

lated from heat transfer coefficient using Lewis relation. Both Dunkle model and Lewis correlation underestimated the water yield for still running under normal and vacuum pressure (see Fig. 6).

4.3. Sensitivity to operational pressure for 3-stage tubular still

Vacuum operation significantly increased the freshwater yield, but a too low pressure might cause adverse effect (see Fig. 7). The sensitivity of fresh water yield on the operational pressure was examined by incrementally varying the P_{op} from 20 kPa to 100 kPa with 2 kPa interval. Other conditions followed the reference case (see §4.1). The maximum fresh water yield of 7.15 kg/m^2 was predicted for $P_{op} = 48$ kPa, which is 19% higher than operating at normal pressure (i.e. 5.81 kg/m^2) and 352% higher than at 20 kPa (i.e. 1.58 kg/m^2).

The P_{op} significantly affects the transient evolution of still temperature, heat absorption and dissipation. Compared with $P_{op} = 48$ kPa, a higher P_{op} (i.e., 90 kPa) leads to higher water temperature in stage 1 (see Fig. 8 (a)), which means a lower temperature difference in between the circulating water and the

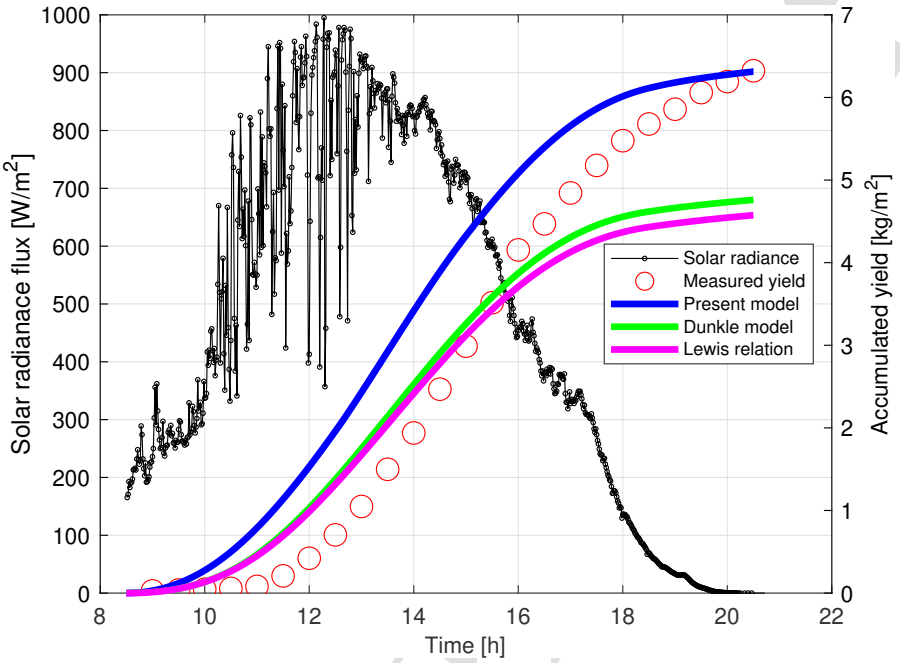

Figure 6: Accumulated yield by the present model compared with other models and experiment, with $P_{op} = 60$ kPa, $G_{max} = 750$ W/m^2 and $R_{sr} = 19.75$ MJ/m^2. The duration time of water yield is 12 hours, i.e., from 8:30 to 20:30.

water at 1st stage. With same solar irradiance, this means a lower energy fed into the still, i.e., a lower $Q_{hu,0}$ for P_{op} higher than 48 kPa (Fig. 8 (c) and (d)). Meanwhile, for $P_{op} = 48$ kPa, a higher mass transfer rate was achieved once the water temperature reaches the saturation temperature which leads to higher outer shell temperature (Fig. 8 (b)). This in turn benefits the dissipation of heat through convection and radiation in last stage (i.e., Q_{dis} Fig. 8 (c) and (d)). Note that there is a lag between Q_{dis} and $Q_{hu,0}$ which is a consequence of vapor transportation within the still. Vapor flows faster at optimal P_{op}, thereby

Journal Pre-proof

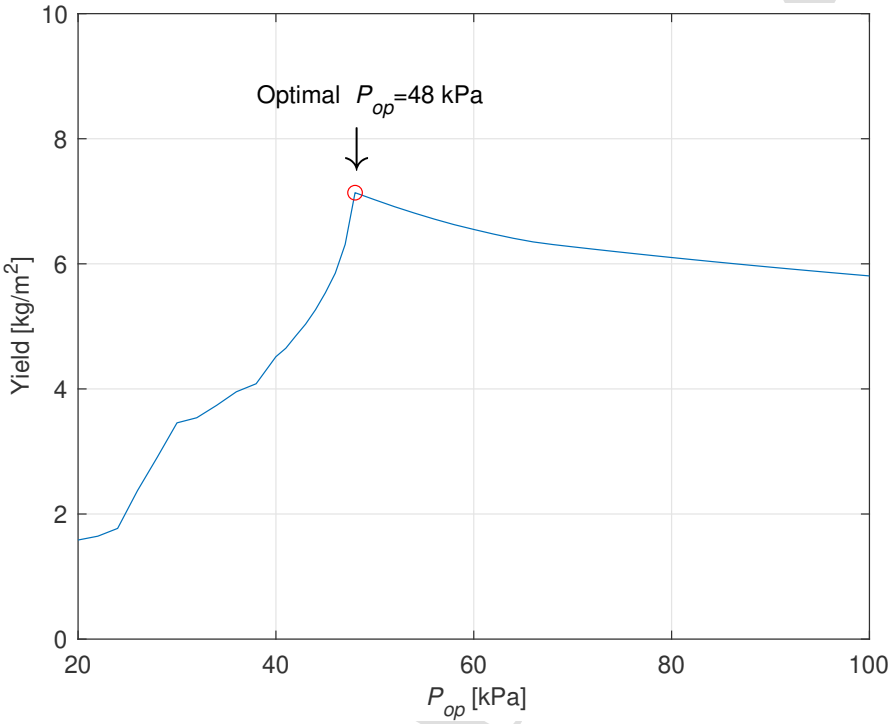

Figure 7: Sensitivity of yield to operational pressure, showing a maximum yield at $P_{op} = 48$ kPa with $G_{max} = 750$ W/m^2 and $R_{sr} = 19.75$ MJ/m^2. The duration time of water yield is 12 hours.

leading to a shorter delaying time with $P_{op} = 48$ kPa than with $P_{op} = 90$ kPa.

A too low P_{op}, on the other hand, jeopardizes this positive feedback and leads to lower fresh water yield. At $P_{op} = 40$ kPa, the temperature of outer shell quickly rose to the saturation temperature of water (see red line in Fig. 8 (b)), led to an uniform temperature field within the still. In this circumstance, there is no temperature gradient between vapor generated and the condense surface. Therefore, the vapor generated in the still can no longer condense on

Journal Pre-proof

any surface. In a vacuum system such as [26], the generated vapor increases the pressure within the still to be above P_{op}, which triggers pump operation and leads to vapor loss. Vapor condensation recurred once the necessary temperature gradient was retained when the temperature of the outer shell drops to certain value lower than the saturation temperature of water. Limited by the water saturation temperature of a low P_{op}, the surface temperature of the outer shell is low which in turn leads to heat transfer deterioration on the outer shell and introduces negative impact on temperature gradient between evaporation and condensation surface. The decreased heat removal rate causes reduction in freshwater yield, as reported in [43]. Under a too low pressure, the still stays in a saturation condition for long duration and produces lower fresh water yield as shown in Fig.7. This phenomenon was previously reported in [32] and in our experimental study [26] where freshwater yield at $P_{op} = 20$ kPa was lower than at the optimum operating pressure, i.e. 40–60 kPa.

At optimal operational pressure, a delicate balance exists in between the energy fed into the system and the energy dissipated through the outer shell, to allow the temperature of outer shell to stay below the saturation temperature whilst maximize the energy absorbed (Fig. 8 (c) and (d)). With $P_{op} = 48$ kPa, the difference of the maximum $Q_{hu,0}$ and Q_{dis} is 1.87 W, whereas with $P_{op} = 90$ kPa this value is 12.2 W.

Journal Pre-proof

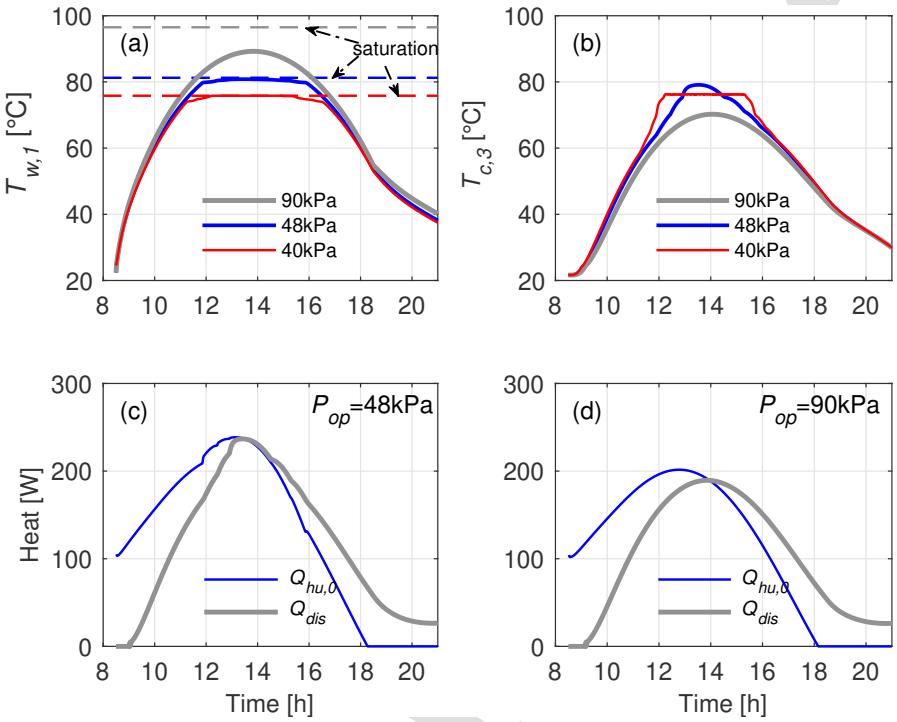

Figure 8: Comparison of $P_{op} = 90$ kPa, $P_{op} = 48$ kPa and $P_{op} = 40$ kPa, showing evolution of: (a), $T_{w,1}$, with horizontal dashed lines indicate the saturation temperature of the corresponding P_{op}; (b) $T_{c,3}$; (c), $Q_{hu,0}$ and Q_{dis} for $P_{op} = 48$ kPa; and (d) $Q_{hu,0}$ and Q_{dis} for $P_{op} = 90$ kPa.

4.4. The effect of solar intensity on still performance

A increasing fresh water yield was predicted at places of greater solar intensity (see Fig. 9). In this section, the G_{max} and P_{op} were systematically varied to investigate the effect of G_{max} and determine the corresponding optimal P_{op}. Other conditions were kept the same as the reference case. With greater G_{max}, more energy was fed into the still, which in turn translated more water into va-

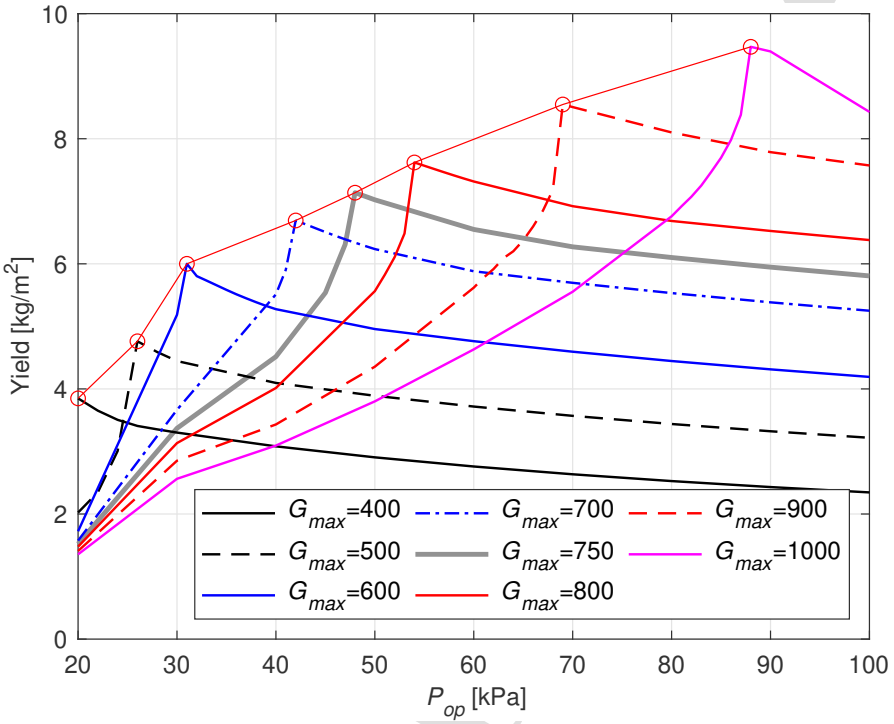

Figure 9: Sensitivity of water yield to solar irradiance. The duration time of water yield is 12 hours.

por. Under $G_{max} = 400$ W/m^2, maximum yield was predicted at $P_{op} = 20$ kPa. There might be higher yield with P_{op} lower than 20 kPa. As the cost required to sustain an extreme low pressure may counteract the higher yield achieved, we chose 20 kPa as the optimal P_{op} for this case. The result at $G_{max} = 400$ W/m^2 also implies that P_{op} would be the lowest operating pressure when input energy is lower than a threshold, i.e., at lower solar irradiation there will not exist any optimum operating pressure and the performance declines at higher operating pressure.

A monotonous increasing optimal P_{op} was predicted for increasing G_{max} (see Fig. 10). This is because the extra energy fed into the still of greater G_{max} imposes higher requirement on heat dissipation. To this end, the temperature of outer shell should be higher to satisfy the heat dissipation efficiency, which means higher optimal P_{op} as it restricts the still temperature. The maximum fresh water yield also increases with higher solar irradiance.

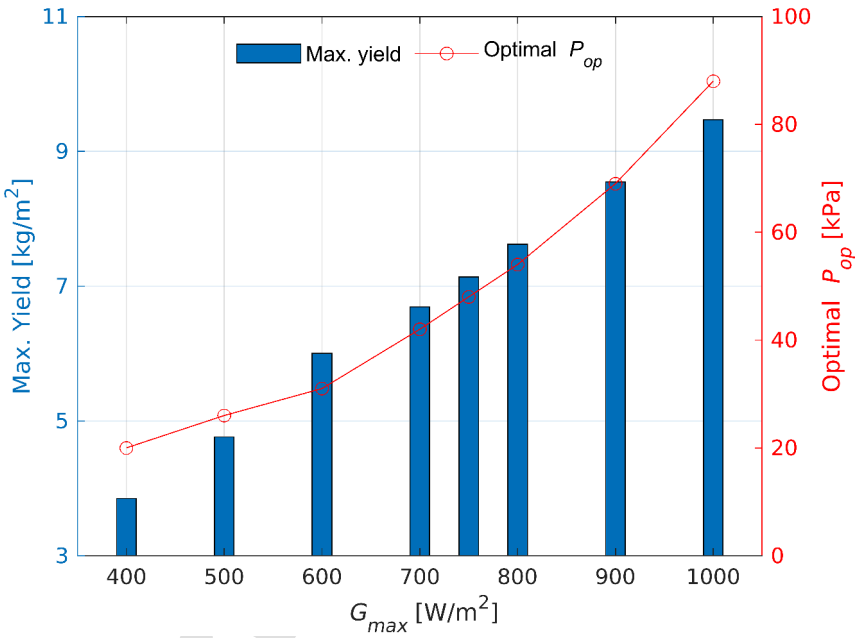

Figure 10: Dependence of maximum water yield and optimal operational pressure on solar irradiance.

Journal Pre-proof

Table 2: Parameters for multi-stage tubular still

Stage	1	2	3	4	5	6
$A_{w,i}$	0.13 m^2	0.16 m^2	0.19 m^2	0.22 m^2	0.25 m^2	0.28 m^2
$A_{c,i}$	0.37 m^2	0.37 m^2	0.37 m^2	0.37 m^2	0.37 m^2	0.37 m^2
M_i	1.5 kg	1.5 kg	1.5 kg	1.5 kg	1.5 kg	1.5 kg

4.5. Dependence of water yield on stage number

Increasing stages is believed to significantly amplify the water yield. Here, the dependence of water yield on stage numbers is examined using the MSSV model. Parameters of the stills were approximated based on the experimental 3-effect still and were listed in Table 2, while other model setting such as solar irradiance and ambient air temperature follow the reference case.

Additional stages amplifies the fresh water yield of the still, with a diminishing marginal effect (Fig. 11). With $P_{op} = 100$ kPa, increasing stages from 1 to 2 produced 1.90 kg/m^2 additional fresh water, whereas increasing from 5 to 6 stages produced only 1.16 kg/m^2 extra water (Fig. 12). The improvement of vacuum operation on water yield is universal to still of all stages. The optimal operational pressures are around $P_{op} = 48$ kPa for all stills, with a minor shift from 48 kPa of 1 stage to 47 kPa of 6 stages. While operating under optimal pressure, water yield of still with 1 stage is 1.11 times than under normal pressure, whereas with 6 stages this value increased to 1.36, suggesting a better improvement of vacuum operation for still with multi-stage.

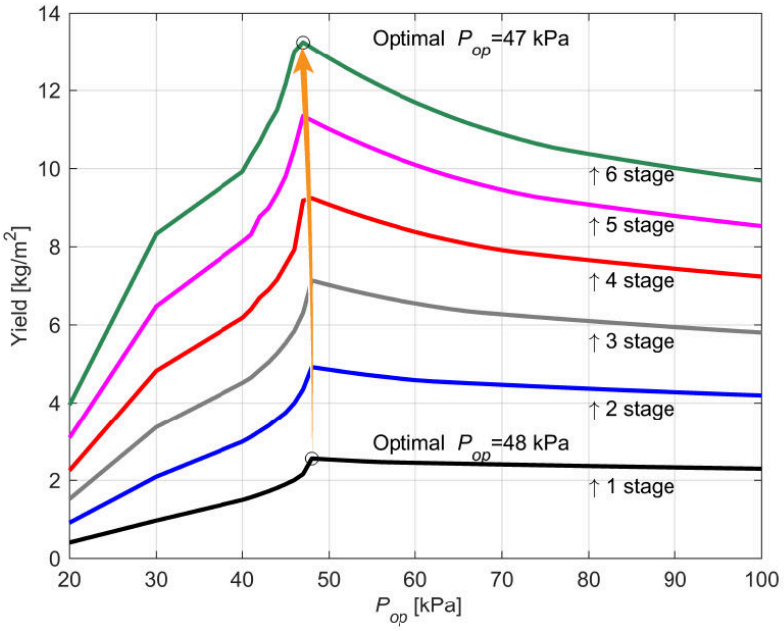

Figure 11: The water yield of multi-stage tubular stills as function of P_{op}. The duration time of water yield is 12 hours.

4.6. Effect of ambient air temperature

The influence of ambient air temperature was examined by setting the ambient air temperature (T_a) to fixed value, i.e., from 0 to 40 ^{o}C. Other settings follow the reference case, i.e., with 3 stages, G_{max} = 750 W/m^2 and A_{co} = 1 m^2. Results show that the water yield increases with T_a for T_a lower than 22 ^{o}C, but decreases for T_a of higher temperature (Fig. 13). Maximum water yield (7.88 kg/m^2) was predicted for T_a = 22 ^{o}C with P_{op} = 30 kPa. Increasing P_{op} was predicted for higher T_a. The temperature of ambient air affects the energy dissipation at both the lowest (Q_{loss}) and last stage (Q_{dis}), as shown in Fig. 14.

Journal Pre-proof

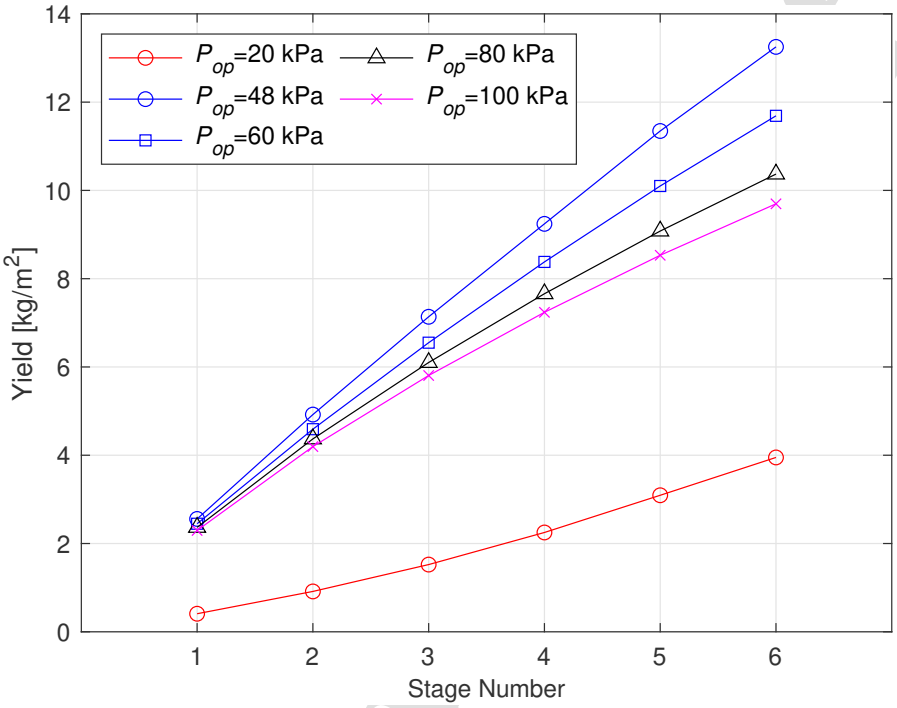

Figure 12: Fresh water yield of mutil-stage tubular still with $G_{max} = 750$ W/m^2 and $R_{sr} = 19.75$ MJ/m^2. The duration time of water yield is 12 hours.

With increasing T_a, Q_{loss} decreases (Fig. 14 a), whereas Q_{dis} increases to a peak value and decline afterwards (Fig. 14 b). Q_{loss} is believed to undermine the still performance as solar energy dissipated at the lowest stage did not participate in the heat transfer within the still, whilst Q_{dis} improves the still performance, as it allows the temperature of outer shell to stay low. Therefore, T_a has complicate influence on the water yield and the optimal operational pressure. The P_{op} corresponding to maximum Q_{dis} coincides with the optimal P_{op} for water yield (Fig. 14 (b)). As illustrated in §4.3, a high energy dissipation at the last stage

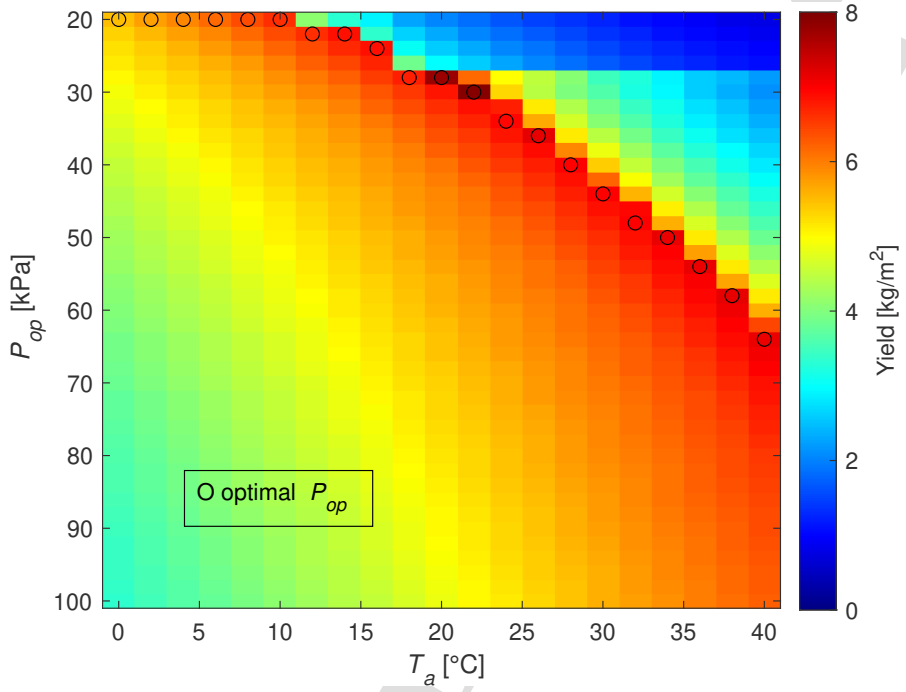

Figure 13: Sensitivity of water yield to the T_a and P_{op}, with $G_{max} = 750$ W/m^2 and $R_{sr} = 19.75$ MJ/m^2. Black circles indicate the P_{op} of maximum water yield for each T_a. The duration time of water yield is 12 hours.

is crucial for the balance of input and output energy in the still.

To amplify the energy dissipation at the last stage whilst prevents energy dissipation at the lowest stage, the water immersion cooling technique is often used in practice [44]. Here, the water immersion cooling technique was simulated by replacing T_a with cooling water temperature (T_{cool}) in the calculation of $Q_{c,s}$ (i.e. Eq. 15) while using T_a value from the reference case in the calculation of $Q_{k,0}$ and $Q_{r,s}$. T_{cool} varies from 2 to 20 ^{o}C. The water yield of immersion cooling is significantly higher than with ambient air cooling (Fig. 15). With T_{cool} and T_a

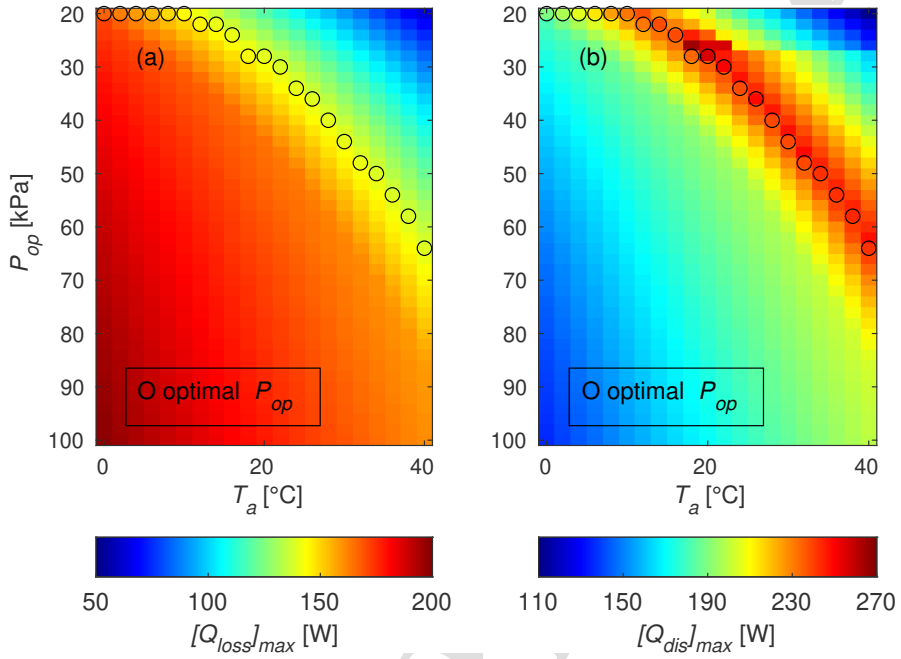

Figure 14: Dependence of energy dissipation at (a) lowest stage and (b) last stage on T_a and P_{op}.

of 2 ^{o}C, yield generate with immersion cooling is 1.65 times of that with ambient air cooling. Maximum water yield (10.51 kg/m^2) was predicted at $T_{cool} = 8$ ^{o}C with $P_{op} = 28$ kPa, which is much higher than the yield generated without the immersion cooling technique (7.15 kg/m^2 as in Fig. 7). The optimal P_{op} with immersion cooling technique is also higher than with ambient air cooling, suggesting less pump energy to maintain vacuum condition. Over cold cooling water such as $T_{cool} < 8$ ^{o}C prevents the still temperature to rise to saturation temperature, therefore generates less yield. Note that the sensitivity analysis present in this section were performed for $G_{max} = 750$ W/m^2. Optimal P_{op}

Journal Pre-proof

519 and maximum water yield would change with other G_{max} value, as indicated in
520 §4.4.

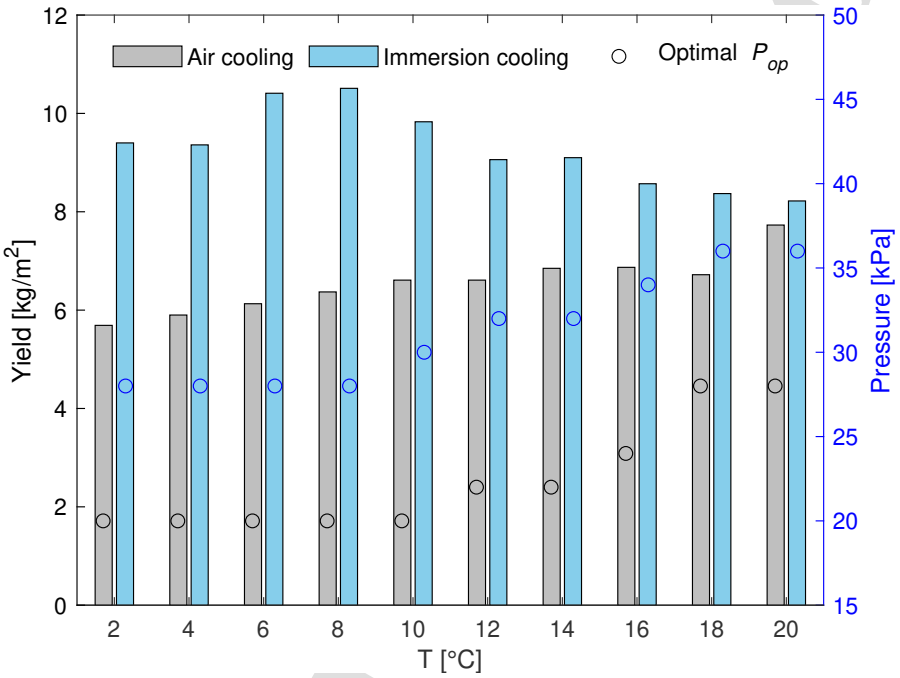

Figure 15: Comparison of water immersion cooling and air cooling, showing the yield and optimal P_{op} of each cooling technique with $G_{max} = 750$ W/m^2 and $R_{sr} = 19.75$ MJ/m^2.

521 5. Discussion

522 *5.1. Extension to multi-stage basin still*

523 The MSSV model was extended to a basin geometry, with parameters ob-
524 tained from literature [30] (listed in Table 3). Other conditions such as the
525 solar irradiance ($G_{max} = 750$ W/m^2), ambient air temperature and solar col-

Journal Pre-proof

Table 3: Parameters for multi-stage basin still

Stage	1	2	3	4	5	6
$A_{w,i}$	0.47 m^2	0.47 m^2	0.47 m^2	0.47 m^2	0.47 m^2	0.47 m^2
$A_{c,i}$	0.47 m^2	0.47 m^2	0.47 m^2	0.47 m^2	0.47 m^2	0.47 m^2
M_i	20 kg	14 kg	14 kg	14 kg	14 kg	14 kg

lector area ($A_{co} = 1$ m^2) were taken from the reference case, so to allow a direct comparison between the tubular and basin still.

Increasing stages of basin still leads to more yield with a reducing marginal benefit, which is similar to the tubular still. The basin still produced less yield than the tubular still. Such difference is bigger for still with multiple stages operating at lower pressure (Fig. 16). A single stage basin still produced approximately 0.15 kg/m^2 less water than a single stage tubular still, whereas with 6-stage the difference is up to 7 kg/m^2 (at $P_{op} = 48$ kPa). Unlike tubular still, water yield of basin still monotonously increases with reducing P_{op} until 20 kPa. One reason might be the heavy weight of water contained in the still (i.e. 14 kg in each stage as shown in Table 3). With same solar irradiance applied, the much more water contained in the basin still lead to slower heat up of water than tubular still, which inhibits the temperature of the basin still to reach a near-saturation state. To have better yielding performance, the basin still needs to be maintained at extremely low pressure. Comparing with a much higher optimal P_{op} of tubular still (i.e. 48 kPa), a much lower P_{op} for basin still (i.e. 20 kPa) poses higher electricity demand for the maintenance of vacuum

Journal Pre-proof

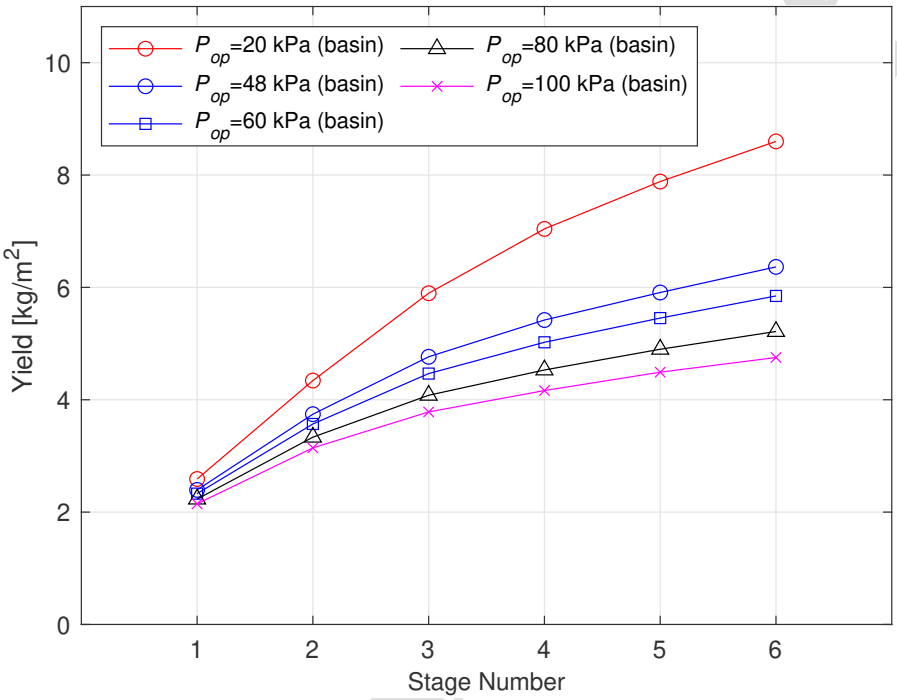

Figure 16: Fresh water yield of multi-stage basin still as function of stage number with G_{max} = 750 W/m^2 and R_{sr} = 19.75 MJ/m^2.The duration time of water yield is 12 hours.

condition.

5.2. Model performance

The MSSV model made use of the diffusion concept of [11] and extended to still of multi-stages. The successful prediction of the high yield of multi-stage still running under vacuum operation has proven the advantage of our model over mathematical models based on Dunkle and Lewis relation. Moreover, a mass transfer formula was proposed for still running under saturation pressure, which improves the model performance while the still reaching boiling tempera-

Journal Pre-proof

ture. The temperature evolution within the still predicted by the present model showed some deviance with measurement, which is due to the ideal settings and calculating deviations from the model. As suggested by Alshammari [45], extending still stage over certain number would probably introduce a hindered effect on heat transfer within the still and lead to adverse impact on water yield of multi-stage still. This effect was not accounted for in the present model and should be considered in future work. The MSSV model was validated against a three-stage tubular solar still running under both normal and vacuum pressure. Note that, a validation for a single-stage solar still had been conducted in our previous study [11]. For wide application of the model, validation with stills of various geometry and stages should be performed.

The MSSV model based on series of experiments with controlled operational pressure using vacuum pump or van [21, 46, 47, 26, 44]. Vacuum regulation with pump or van may cause vapor loss, especially in the circumstance of water saturation. A possible solution would be a non-interference vacuum operation system which sets an initial vacuum pressure but relaxes the pressure control afterward. The pressure within the still after the initial setting would be a dependent variable according to the operating temperatures. To the best of authors' knowledge, such operation system was rarely reported and would require a sophisticated and innovative control system. For the next step, we would like to test the solar still with non-interference vacuum operation and develop a corresponding predictive model.

Journal Pre-proof

6. Conclusion

A predictive model for the yield of multi-stage tubular solar still (MSSV) was developed, which accounts for the high mass transfer rate under vacuum operation and near saturation condition. The MSSV model successfully reproduced the field experiments of a 3-stage tubular still operating under both normal and vacuum condition and precisely predicted the temperature and water yield evolution. Under typical weather, i.e., with $G_{max} = 750$ W/m^2, 19.75 MJ/m^2 cumulative solar radiation and $T_a \approx 20$ ^{o}C, the optimal P_{op} of a 3-stage tubular still was identified to as 48 kPa. Maximum water yield (7.15 kg/m^2) was obtained at the optimal P_{op}, which is 19% higher than running at normal pressure (5.81 kg/m^2) and 352% higher than at 20 kPa (1.58 kg/m^2). In this circumstance, the solar still achieved a delicate balance between the energy adsorbed by the still and the energy dissipated.

The solar still performance and the optimal P_{op} were affected by solar intensity, stage numbers and cooling technique. A greater solar irradiance led to more water yield and higher optimal P_{op}. Increasing the stage number improved the fresh water yield with diminishing marginal effect, and slightly shift the optimal P_{op} to a lower value. In choosing a suitable stage number for multiple stage still, the cost of manufacture and vacuum maintenance should also be considered. With water immersion cooling, a 3-stage tubular still generated 10.51 kg/m^2 fresh water (with $P_{op} = 28$ kPa and $T_{cool} = 8^o$C), accounting for a 47% increase than that with air cooling (7.15 kg/m^2). The MSSV model has

Journal Pre-proof

proven its ability in identifying optimal P_{op} and could serve as a design tool for the operation of multi-stage still with both basin and tubular geometry.

Nomenclature

Greek symbol

β	expansion coefficient, K^{-1}
δ	wall thickness, m
ϵ	emissivity of the surfaces
η_{co}	efficiency of the solar collector
λ	thermal conductivity, $W.m^{-1}.K^{-1}$
μ	dynamic viscosity, $kg.m^{-1}.s^{-1}$
ρ	density, $kg.m^{-3}$
σ	Stefan-Boltzmann constant, 5.67×10^{-8} $W.m^{-2}.K^{-4}$

Other symbol

d	diameter of tube, m
$\Delta T'$	revised temperature difference, K
ΔT	temperature difference, K
$\dot{m}_e$	distillate rate per square meter, $kg.s^{-1}.m^{-2}$

Journal Pre-proof

612	$\dot{m}_{e,1}$	distillate rate under normal pressure, kg.s^{-1}.m^{-2}
613	$\dot{m}_{e,2}$	distillate rate under saturation pressure, kg.s^{-1}.m^{-2}
614	A	area, m^2
615	A_c	heat convective area, m^2
616	C	numerical constant
617	c_p	specific heat at constant pressure, J.kg^{-1}·K^{-1}
618	C_{mb}	saturation coefficient
619	D	mass diffusion coefficient, m^2.s^{-1}
620	D_0	mass diffusion coefficient of vapour at atmospheric pressure and, $T_a = 25$
621		^oC, 0.256×10^{-4}m^2.s^{-1}
622	G	solar irradiance, W.m^{-2}
623	g	gravity acceleration, 9.8 m.s^{-2}
624	G_{max}	maximum solar irradiance, W.m^{-2}
625	Gr	Grashof number
626	H	average solar irradiance during the day, W.m^{-2}
627	h_c	convective heat transfer coefficient, W.m^{-2}.K^{-1}
628	h_e	evaporative heat transfer coefficient, W.m^{-2}.K^{-1}
629	h_{fg}	latent heat of water vapourization, 2.3×10^6 kJ.kg^{-1}

Journal Pre-proof

Journal Pre-proof

630	h_m	mass transfer coefficient, m.s^{-1}
631	L	average distance between the evaporation and condensation surface, m
632	M	weight of water in trough, kg
633	M_a	the molar mass of air, 28.96 kg.kmol^{-1}
634	M_m	the molar mass of humid air, kg.kmol^{-1}
635	M_v	the molar mass of water vapour, 18 kg.kmol^{-1}
636	P	pressure, kPa
637	P_0	atmospheric pressure, 101 kPa
638	P_a	partial air pressure, kPa
639	P_c	partial pressure of vapour near the condensation surface, kPa
640	P_{LM}	logarithmic mean partial pressure, kPa
641	P_{op}	operating pressure, kPa
642	P_{sv}	saturation pressure, kPa
643	P_v	partial vapour pressure in humid air, kPa
644	P_w	partial pressure of vapour near the free liquid surface, kPa
645	Pr	Prandtl number
646	Q_c	convective heat transfer rate, W
647	Q_e	evapourative heat transfer rate, W

Journal Pre-proof

648	Q_h	input heat rate, W
649	Q_k	heat loss, W
650	Q_r	radiant heat transfer rate, W
651	Q_{dis}	energy dissipation rate at last stage, W
652	$Q_{h,0}$	collected solar power, W
653	Q_{hu}	effective heating power, W
654	Q_{loss}	energy dissipation rate at lowest stage (exterior of the solar still), W
655	$Q_{r,s}$	radiant heat transfer rate between the shell and ambient environment,
656		W
657	R	universal gas constant, 8.314 J.mol^{-1}.K^{-1}
658	R_1	thermal resistance of insulation layer, K.W^{-1}
659	R_2	thermal resistance of outwall radiation, K.W^{-1}
660	R_3	thermal resistance of outwall convection, K.W^{-1}
661	R_{sr}	cumulative solar radiation, MJ.m^{-2}
662	Re	Reynolds number
663	RH	relative humidity
664	Sc	Schmidt number
665	Sh	Sherwood number

Journal Pre-proof

Journal Pre-proof

666	T	temperature, K
667	t	time, s
668	T_a	temperature of the ambient environment, K
669	t_a	sunrise time, s
670	t_b	sunset time, s
671	T_{sky}	the sky temperature, K
672	$T_{w,s}$	saturation temperature of water, K
673	V_w	wind speed, m.s^{-1}

674 **Subscript**

675	a	dry air
676	c	condensation surface
677	co	solar collector
678	es	surface of exchange tube
679	i	stage, i=0 correlates to the circulating water
680	ins	insulation layer
681	m	humid air, mixture
682	s	tubular shell
683	v	vapour
684	w	water

Journal Pre-proof

Journal Pre-proof

Acknowledgements

We gratefully acknowledge the financial support for this research provided by the National Natural Science Foundation of China (Nos. 51606130). We sincerely appreciate all valuable comments and suggestions from anonymous reviewers.

References

[1] N. Xu, J. Li, Y. Wang, C. Fang, X. Li, Y. Wang, L. Zhou, B. Zhu, Z. Wu, S. Zhu, J. Zhu, A water lily–inspired hierarchical design for stable and efficient solar evaporation of high-salinity brine. science advances, Science Advances 5 (7) (2019) eaaw7013. doi:10.1126/sciadv.aaw7013.

[2] U. W. W. A. Programme, The United Nations world water development report 2021: valuing water, United Nations Educational, Scientific and Cultural Organization, Paris, 2021.

[3] A. Al-Karaghouli, D. Renne, L. L. Kazmerski, Technical and economic assessment of photovoltaic-driven desalination systems, Renewable Energy 35 (2) (2010) 323–328. doi:10.1016/j.renene.2009.05.018.

[4] S. Lee, J. Hong, D. Har, Jointly optimized control for reverse osmosis desalination process with different types of energy resource, Energy 117 (2016) 116–130. doi:10.1016/j.energy.2016.10.078.

[5] A. Kasaeian, F. Rajaee, W.-M. Yan, Osmotic desalination by solar

Journal Pre-proof

energy: A critical review, Renewable Energy 134 (2019) 1473–1490. doi:10.1016/j.renene.2018.09.038.

[6] M. Talaat, M. Awad, E. Zeidan, A. Hamed, Solar-powered portable apparatus for extracting water from air using desiccant solution, Renewable Energy 119 (2018) 662–674. doi:10.1016/j.renene.2017.12.050.

[7] M. Elashmawy, An experimental investigation of a parabolic concentrator solar tracking system integrated with a tubular solar still, Desalination 411 (2017) 1–8. doi:10.1016/j.desal.2017.02.003.

[8] L. Zhou, Y. Tan, J. Wang, W. Xu, Y. Yuan, W. Cai, S. Zhu, J. Zhu, 3D self-assembly of aluminium nanoparticles for plasmon-enhanced solar desalination, Nature Photonics 10 (6) (2016) 393–398. doi:10.1038/nphoton.2016.75.

[9] P. Durkaieswaran, K. K. Murugavel, Various special designs of single basin passive solar still – a review, Renewable and Sustainable Energy Reviews 49 (2015) 1048–1060. doi:10.1016/j.rser.2015.04.111.

[10] L. Sahota, Shyam, G. Tiwari, Analytical characteristic equation of nanofluid loaded active double slope solar still coupled with helically coiled heat exchanger, Energy Conversion and Management 135 (2017) 308–326. doi:10.1016/j.enconman.2016.12.078.

[11] G. Xie, L. Sun, T. Yan, J. Tang, J. Bao, M. Du, Model development and experimental verification for tubular solar still operating under vacuum condition, Energy 157 (2018) 115–130. doi:10.1016/j.energy.2018.05.130.

Journal Pre-proof

[12] L. Sahota, G. Tiwari, Effect of nanofluids on the performance of passive double slope solar still: A comparative study using characteristic curve, Desalination 388 (2016) 9–21. doi:10.1016/j.desal.2016.02.039.

[13] A. Elfasakhany, Performance assessment and productivity of a simple-type solar still integrated with nanocomposite energy storage system, Applied Energy 183 (2016) 399–407. doi:10.1016/j.apenergy.2016.09.002.

[14] N. Fadaei, A. Kasaeian, A. Akbarzadeh, S. H. Hashemabadi, Experimental investigation of solar chimney with phase change material (pcm), Renewable Energy 123 (2018) 26–35. doi:10.1016/j.renene.2018.01.122.

[15] S. Khanmohammadi, S. Khanmohammadi, Energy, exergy and exergo-environment analyses, and tri-objective optimization of a solar still desalination with different insulations, Energy 187 (2019) 115988. doi:10.1016/j.energy.2019.115988.

[16] M. S. Yousef, H. Hassan, Energetic and exergetic performance assessment of the inclusion of phase change materials (pcm) in a solar distillation system, Energy Conversion and Management 179 (2019) 349–361. doi:10.1016/j.enconman.2018.10.078.

[17] P. Tao, G. Ni, C. Song, W. Shang, J. Wu, J. Zhu, G. Chen, T. Deng, Solar-driven interfacial evaporation, Nature Energy 3 (12) (2018) 1031–1041. doi:10.1038/s41560-018-0260-7.

[18] H. Ambarita, Study on the performance of natural vacuum desalination

Journal Pre-proof

748 system using low grade heat source, Case Studies in Thermal Engineering
749 8 (2016) 346–358. doi:10.1016/j.csite.2016.09.005.

750 [19] S.-H. Choi, Thermal type seawater desalination with barometric vacuum and solar energy, Energy 141 (2017) 1332–1349.
752 doi:10.1016/j.energy.2017.11.007.

753 [20] Y. A. Abakr, A. F. Ismail, Theoretical and Experimental Investigation of
754 a Novel Multistage Evacuated Solar Still , Journal of Solar Energy Engi-
755 neering 127 (3) (2005) 381–385. doi:10.1115/1.1866145.

756 [21] M. Ahmed, M. Hrairi, A. Ismail, On the characteristics of multistage
757 evacuated solar distillation, Renewable Energy 34 (6) (2009) 1471–1478.
758 doi:10.1016/j.renene.2008.10.029.

759 [22] A. G. Ibrahim, E. E. Allam, S. E. Elshamarka, A modified basin type solar
760 still: Experimental performance and economic study, Energy 93 (2015)
761 335–342. doi:10.1016/j.energy.2015.09.045.

762 [23] I. Hamawand, L. Lewis, N. Ghaffour, J. Bundschuh, Desalination of salty
763 water using vacuum spray dryer driven by solar energy, Desalination 404
764 (2017) 182–191. doi:10.1016/j.desal.2016.11.015.

765 [24] Z. Omara, A. Kabeel, F. Essa, Effect of using nanofluids and providing
766 vacuum on the yield of corrugated wick solar still, Energy Conversion and
767 Management 103 (2015) 965–972. doi:10.1016/j.enconman.2015.07.035.

768 [25] T. Yan, G. Xie, H. Liu, Z. Wu, L. Sun, CFD investigation of va-

Journal Pre-proof

por transportation in a tubular solar still operating under vacuum, International Journal of Heat and Mass Transfer 156 (2020) 119917. doi:10.1016/j.ijheatmasstransfer.2020.119917.

[26] G. Xie, W. Chen, T. Yan, J. Tang, H. Liu, S. Cao, Three-effect tubular solar desalination system with vacuum operation under actual weather conditions, Energy Conversion and Management 205 (2020) 112371. doi:10.1016/j.enconman.2019.112371.

[27] G. Xie, L. Sun, Z. Mo, H. Liu, M. Du, Conceptual design and experimental investigation involving a modular desalination system composed of arrayed tubular solar stills, Applied Energy 179 (2016) 972–984. doi:10.1016/j.apenergy.2016.07.057.

[28] V. G. Gude, N. Nirmalakhandan, S. Deng, A. Maganti, Feasibility study of a new two-stage low temperature desalination process, Energy Conversion and Management 56 (2012) 192–198. doi:10.1016/j.enconman.2011.11.026.

[29] H. Zheng, Z. Chang, Z. Chen, G. Xie, H. Wang, Experimental investigation and performance analysis on a group of multi-effect tubular solar desalination devices, Desalination 311 (2013) 62–68. doi:10.1016/j.desal.2012.11.021.

[30] M. K. Estahbanati, M. Feilizadeh, K. Jafarpur, M. Feilizadeh, M. R. Rahimpour, Experimental investigation of a multi-effect active solar still: The effect of the number of stages, Applied Energy 137 (2015) 46–55. doi:10.1016/j.apenergy.2014.09.082.

Journal Pre-proof

[31] P. V. Kumar, A. K. Kaviti, O. Prakash, K. S. Reddy, Optimization of design and operating parameters on the year round performance of a multi-stage evacuated solar desalination system using transient mathematical analysis, International Journal of Energy and Environment 3 (2012) 409–434.

[32] K. Reddy, K. R. Kumar, T. S. O'Donovan, T. Mallick, Performance analysis of an evacuated multi-stage solar water desalination system, Desalination 288 (2012) 80–92. doi:10.1016/j.desal.2011.12.016.

[33] K. Reddy, H. Sharon, Active multi-effect vertical solar still: Mathematical modeling, performance investigation and enviro-economic analyses, Desalination 395 (2016) 99–120. doi:10.1016/j.desal.2016.05.027.

[34] G. Xie, J. Xiong, H. Liu, B. Xu, H. Zheng, Y. Yang, Experimental and numerical investigation on a novel solar still with vertical ripple surface, Energy Conversion and Management 98 (2015) 151–160. doi:10.1016/j.enconman.2015.03.099.

[35] A. Ahsan, T. Fukuhara, Mass and heat transfer model of tubular solar still, Solar Energy 84 (7) (2010) 1147–1156. doi:10.1016/j.solener.2010.03.019.

[36] G. Xiao, X. Wang, M. Ni, F. Wang, W. Zhu, Z. Luo, K. Cen, A review on solar stills for brine desalination, Applied Energy 103 (2013) 642–652. doi:10.1016/j.apenergy.2012.10.029.

[37] R. S. Adhikari, A. Kumar, A. Kumar, Estimation of mass-transfer rates in solar stills, International Journal of Energy Research 14 (7) (1990) 737–744. doi:10.1002/er.4440140705.

Journal Pre-proof

[38] J. Holman, Heat Transfer, 10th Edition, McGraw-Hill Education, New York, 2010.

[39] R. Dunkle, Solar water distillation: the roof type still and the multiple effect diffusor, in: Proc. of International Heat Transfer, V, University of Colorado, 1961, p. 895.

[40] N. Rahbar, J. Esfahani, Productivity estimation of a single-slope solar still: Theoretical and numerical analysis, Energy 49 (2013) 289–297. doi:10.1016/j.energy.2012.10.023.

[41] P. Tsilingiris, Modeling heat and mass transport phenomena at higher temperatures in solar distillation systems – the chilton–colburn analogy, Solar Energy 84 (2) (2010) 308–317. doi:10.1016/j.solener.2009.11.012.

[42] P. Tsilingiris, The influence of binary mixture thermophysical properties in the analysis of heat and mass transfer processes in solar distillation systems, Solar Energy 81 (12) (2007) 1482–1491. doi:10.1016/j.solener.2007.02.005.

[43] M. Saad, M. Ahmed, V. M. Morcos, Performance analysis of a vacuum desalination system, Vol. Volume 1: Advances in Aerospace Technology; Energy Water Nexus; Globalization of Engineering; Posters of ASME International Mechanical Engineering Congress and Exposition, 2011, pp. 421–425. doi:10.1115/IMECE2011-62655.

[44] T. Yan, G. Xie, W. Chen, Z. Wu, J. Xu, Y. Liu, Experimental study on three-effect tubular solar still under vacuum and immersion cooling, Desalination 515 (2021) 115211. doi:10.1016/j.desal.2021.115211.

Journal Pre-proof

[45] F. Alshammari, M. Elashmawy, M. M. Ahmed, Cleaner production of freshwater using multi-effect tubular solar still, Journal of Cleaner Production 281 (2021) 125301. doi:10.1016/j.jclepro.2020.125301.

[46] A. Kabeel, Z. Omara, F. Essa, Enhancement of modified solar still integrated with external condenser using nanofluids: An experimental approach, Energy Conversion and Management 78 (2014) 493–498. doi:10.1016/j.enconman.2013.11.013.

[47] T. Yan, G. Xie, L. Sun, M. Du, H. Liu, Experimental investigation on a two-effect tubular solar still operating under vacuum conditions, Desalination 468 (2019) 114057. doi:10.1016/j.desal.2019.06.023.

Journal Pre-proof

Journal Pre-proof

CRediT authorship contribution statement

Wen Long Chen: Conceptualization, Methodology, Simulation, Investigation, Writing - original draft. Guo Xie: Conceptualization, Methodology, Investigation, Writing - original draft.

Journal Pre-proof

Journal Pre-proof

Declaration of interests

☒ The authors declare that they have no known competing financial interests or personal relationships that could have appeared to influence the work reported in this paper.

☐ The authors declare the following financial interests/personal relationships which may be considered as potential competing interests:

Journal Pre-proof

https://dspace.org/

Performance of multi-stage tubular solar still operating under vacuum

Chen, Wenlong; Xie, Guo

2022-11-21
Elsevier
https://doi.org/10.1016/j.renene.2022.11.023
Chen WL, Xie G. (2022) Performance of multi-stage tubular solar still operating under vacuum. Renewable Energy, Volume 201, Part 2, December 2022, pp. 34-46

Downloaded from a DSpace repository. https://dspace.org/